

A Method for Thermal Diffusivity Determination of Thermal Insulators

Jozef Gembarovic · Raymond E. Taylor

Published online: 11 October 2007
© Springer Science+Business Media, LLC 2007

Abstract A so-called “three-point” (3P) method has been developed for thermal diffusivity measurements of thermal insulating materials. One side of a cylindrical specimen, sandwiched between two thin metal plates, is subjected to intense light from an incandescent lamp to generate a thermal perturbation. The temperature response is measured in three locations along the test specimen. Thermocouples are located at the front and rear faces of the specimen, and the third is placed inside the specimen at a known location. The two outside temperatures are used as boundary conditions, and the unknown thermal diffusivity is calculated from the third temperature versus time curve. The method combines the advantages of rapid transient non-contact heating methods with the well-defined boundary conditions of steady-state methods. The results of the 3P method are compared with those from steady-state methods for a micro-porous insulation material and for a honeycomb structure.

Keywords Thermal conductivity · Thermal diffusivity · Thermal insulation · Transient method

1 Introduction

The thermal conductivity of thermal insulations is usually measured using steady-state methods, e.g., guarded hot-plate (GHP) method [1], heat flow meter technique [2, 3], etc. These methods are well established, highly standardized, and reasonably precise in the temperature range from -50 to 600°C . Obvious disadvantages of the steady-state methods are the need for large samples and long measurement times (sometimes

J. Gembarovic (✉) · R. E. Taylor
Thermophysical Properties Research Laboratory, Inc., 3080 Kent Avenue, West Lafayette, IN 47906,
USA
e-mail: gembar@tpri.com

days). Rapid transient methods (e.g., flash method [4], hot-wire method [5], transient hot strip, transient hot-disc method [6], etc.), which in the last 50 years have almost completely replaced the older steady-state methods and become the dominant means to determine the thermal conductivity of many types of solid materials, are seldom used for thermal insulations, despite the fact that they use much smaller samples, the measurement takes only minutes, and they can be applied to a broader range of temperatures. Application of the transient methods to thermal insulations is hampered by multicomponent heat transfer and structural complexity and diversity of today's commonly used thermal insulations. Poorly conducting, transparent non-homogeneous samples with ill-defined surfaces, such as loosely packed fibrous materials, porous insulations, aerogels, etc., still present real challenges for experimenters.

For more than 30 years, we have specialized in developing and using the transient thermal diffusivity measurement to determine the thermal conductivity of thermal insulations. First, we modified the laser flash technique by substituting step heating for flash heating, i.e., replacing the laser with a lamp or film heater. In the step-heat technique, presented by Bittle and Taylor [7], a constant heat flux condition was imposed on the front surface of the sample and the rear surface was considered to be adiabatic. The thermal diffusivity was calculated from collected temperature–time data and the corresponding solution of the heat equation using parameter estimation methods. The samples used in the method were relatively larger than the laser flash samples, but small compared to guarded hot-plate samples.

The step-heat method was later modified for fibrous insulations [8]. The constant heat flux condition on the front surface and the adiabatic condition on the rear surface were replaced by measured time–temperature curves. The sample temperatures were measured at the front and rear faces of the specimen and in one or two known locations within the sample. The sample, of the size of the typical step-heat sample, was sandwiched between two thin metal plates of diameter equal to the sample diameter. The plates provided sample support, absorbed the light used to heat the sample, and secured the thermocouple's position and contact with the sample material. The temperature–time data from the internal thermocouples were then used to calculate the thermal diffusivity of the sample using a parameter-estimation method. Boundary temperature data were used to calculate the temperature distribution in the sample using a one-dimensional Crank-Nicholson finite-difference scheme.

The number of thermocouples used in the modified step-heat method was later reduced to three, and the apparatus described in [8] was redesigned for measurements in vacuum or special atmospheres. The procedure of the thermal-diffusivity measurement was described in [9]. A digital multimeter in combination with a pc was used to read and record the various temperatures inputs. Two incandescent lamps were used for the radiant heating of the sample. This significantly improved the accuracy and reliability of the results, especially at higher temperatures.

This article summarizes further developments and improvements to the method for use in high-temperature thermal-diffusivity measurements of thermal insulation. In order to differentiate between the earlier versions, we will call it the three-point (3P) method in this article. Some of the 3P method results are compared with those from the steady-state methods.

2 Method Development

2.1 Theory

The temperature distribution $T(z, t)$, $0 \leq z \leq L$, $t > 0$, in a homogeneous and isotropic sample (depicted in Fig. 1), with constant thermophysical properties, initially at temperature T_0 , is a solution of the one-dimensional heat conduction problem with boundary conditions of the first kind:

$$a \frac{\partial^2 T}{\partial z^2} = \frac{\partial T}{\partial t}, \quad T(z, 0) = T_0, \quad T(0, t) = \phi_1(t), \quad T(L, t) = \phi_2(t), \quad (1)$$

where a is the effective thermal diffusivity and $\phi_j(t)$, ($j = 1, 2, 3$) are the temperature responses of the j -th thermocouple. The analytical solution of Eq. 1 is given by the formula [10],

$$T(z, t) = T_0 + \frac{2a\pi}{L^2} \sum_{n=1}^{\infty} n e^{-an^2\pi^2 t/L^2} \sin \frac{n\pi z}{L} \int_0^t e^{an^2\pi^2 x/L^2} [\varphi_1(x) - (-1)^n \varphi_2(x)] dx \quad (2)$$

Since the analytical solution, given by Eq. 2, is not practical for numerical calculations, our recently published damped heat wave (DHW) algorithm [11] is used to calculate the temperature within the sample. The DHW algorithm is more precise and more stable than the finite difference scheme used in the modified step-heat method. In the DHW algorithm, a finite homogeneous medium of thickness L is divided into N equal slabs of thickness $\Delta l = L/N$. These slabs are replaced by a perfect conductor of the same heat capacity separated by the thermal resistance $\Delta l/\lambda$ (where λ is the thermal conductivity of the medium), so the temperature within a slab at any given time is constant. Heat propagates through the medium due to a temperature difference between the slabs. A certain portion (given by the inner transfer coefficient ξ) of the excessive heat energy moves from one slab to the next, thus lowering the temperature difference between the two neighboring slabs. This redistribution process (the damped heat wave) starts from the left boundary slab and marches in space from one pair of slabs to another. When the wave reaches the boundary of the medium, it bounces back and moves in the opposite direction in a perpetual manner. Slab temperatures are $T_{i,m} = T(x_i, t_m)$, where x_i ($i = 0, 1, 2, \dots, N-1$) is a spatial point (middle of the i -th slab) and $t_m = m\Delta t$, ($m = 0, 1, 2, \dots$) is a discrete time point. The temperatures of the boundary slabs change only after the heat wave finishes one whole loop; therefore, the time step Δt is equal to one loop time interval. The time step Δt is thus divided into $2N$ sub-steps. Despite the almost trivial simplicity of this algorithm, the temperature distribution in the medium at time t_{m+1} as a function of the temperature distribution at t_m is expressed by rather lengthy and complicated formulae [12]:

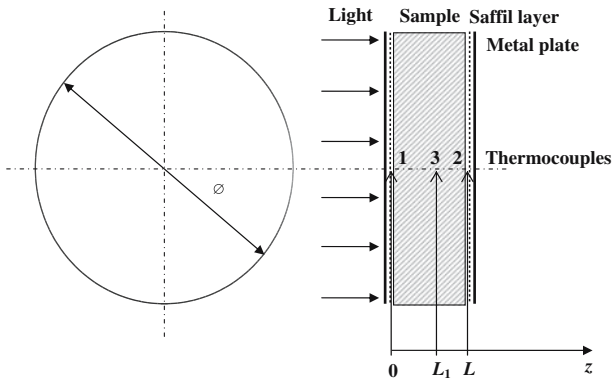


Fig. 1 Diagram of the sample and measurement geometry

$$T_{0,m+1} = \left[2 \frac{1 + \xi^{2N-1}}{1 - \xi} - 1 \right] T_{0,m} + 2 \frac{1 - \xi}{1 + \xi} \sum_{j=1}^{N-1} \xi^j \left(1 + \xi^{2(N-j)-1} \right) T_{j,m}, \quad (3)$$

$$\begin{aligned} T_{i,m+1} = & 2 \frac{1 - \xi}{1 + \xi} \left(1 + \xi^{2(N-i)-3} \right) \sum_{j=0}^{i-1} \xi^j (1 - \xi)^j T_{j,m} \\ & + \left[(1 - \xi)^2 \left(2 \frac{1 + \xi^{2(N-i)-3}}{1 + \xi} - 1 \right) + \xi^2 \right] T_{i,m} \\ & + 2 \frac{(1 - \xi)^2}{1 + \xi} \sum_{j=0}^{N-i-2} \xi^j \left(1 + \xi^{2(N-i-j)+1} \right) T_{j+i+1,m}, \end{aligned} \quad (4)$$

for $i = 1, 2, \dots, N - 1$.

The inner transfer coefficient ξ is a dimensionless quantity given by

$$\xi = \frac{\mu}{\mu + 2}, \quad (5)$$

where

$$\mu = \frac{a \Delta t}{(\Delta l)^2}, \quad (6)$$

is the mesh ratio and a is the thermal diffusivity of the material.

The effective thermal diffusivity a of the sample is calculated from the interior position (thermocouple at $z = L_1$) temperature data $\phi_3(t_m)$, which are compared to the solution of the direct heat conduction problem $T(L_1, t_m)$. A standard software package DODRPACK Version 2.1 [13] is used for the thermal-diffusivity calculation using an ordinary least-squares method.

The thermal conductivity λ of the sample material is then calculated using

$$\lambda = \rho c_p a, \quad (7)$$

where ρ is the bulk density and c_p is the specific heat at constant pressure.

2.2 Experimental

2.2.1 Apparatus Description

The 3P method apparatus consists of a vacuum chamber with two quartz glass windows. A regulated dc power supply (Agilent 6671A) is used for the stainless steel furnace tube heating element. A 600 W quartz-iodide, tungsten element bulb, mounted outside the chamber within an aluminum parabolic reflector, is used as the heat source. The flux intensity was measured 300 mm from the bulb and found to vary less than 2% across a 50-mm diameter.

The experimental data are collected using a multi-channel A/D converter with 12-bit resolution and direct thermocouple inputs. The sample temperature is measured using chromel-alumel thermocouples (thickness, 7.62×10^{-2} mm). The experiment is controlled, and data are collected using a software package developed by TPRL, Inc.

A cylindrical sample of 50 mm diameter and 10 mm thickness is sandwiched between two thin metal plates (see Fig. 1). The plates support the sample and prevent light from penetrating into the sample material. Thin Saffil screens inserted between the sample and metal plates insulate the sample material and the surface thermocouples from the metal plates.

2.2.2 Procedures

It has to be noted that $\phi_1(t)$ and $\phi_2(t)$ at the sample boundaries in Eq. 1 are arbitrary functions of time. From the experimental point of view, it means that we do not need to generate a particular shape of heat pulse. Any thermal disturbance, (arbitrary heat pulse), strong enough to generate a transient state reliably detected by the thermocouples in the sample can be utilized for the thermal diffusivity determination. The disturbance should not be too strong, in order not to overheat the sample and to keep valid the assumption of constant thermal properties during the test. Contrary to the step-heating method and the laser flash method, there is no need for the disturbance to start at a well-known time and there is also no need for the sample surfaces to be thermally insulated from the surroundings. The lamp can be turn on and off at any time and the only requirement for the data acquisition system is to record the sample temperatures with no relative delays between the thermocouples.

From the nature of the heat conduction formulation, it follows that the thermocouples 1 and 2 need not to be placed exactly at the physical boundaries of the sample. All three thermocouples should be at the same radial position (preferably on the main axis), but at different axial positions within the sample. Only relative axial distances between them enter into the diffusivity calculation.

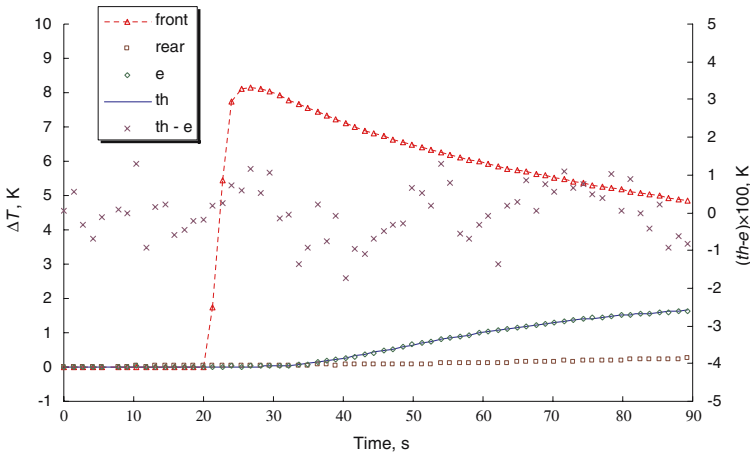


Fig. 2 Typical temperature response curves (“front” is the temperature at front sample surface; “rear” is the temperature at rear sample surface; “e” is the temperature of the third thermocouple; “th” is the theoretically calculated temperature; and “th – e” are the residuals (in percent)—right axis)

Before the diffusivity measurement, the sample is usually evacuated inside the vacuum chamber for about 1 h in order to dry the sample material. Then the chamber is filled with a gas, and the sample temperature is stabilized at $\sim 23^\circ\text{C}$ for 1 h. Nitrogen is often used instead of air in order to prevent corrosion of our stainless steel furnace element at higher temperatures. Thermal diffusivity values measured in nitrogen are the same as in air, within the experimental uncertainty of the 3P method.

The steady-state (baseline) sample temperature is recorded in the first 20 s, and then the incandescent lamp is turned on for a period up to 10 s to generate a test heat pulse. Actual measurement time ranges from 60 to 450 s and depends on the sample thickness and the thermal diffusivity of the sample material. The maximum temperature rise at the irradiated sample boundary is $\sim 10\text{ K}$. The inside thermocouple rise due to the pulse is about 1 K. The opposite boundary temperature rise is only of order 0.1 K. Typical temperature response curves for an insulation sample (diameter $\varnothing = 48.0\text{ mm}$, thickness $L = 12.85\text{ mm}$, $L_1 = 6.435\text{ mm}$, $T_0 = 23^\circ\text{C}$) are shown in Fig. 2. The differences between the theoretical curve with $a = 2.36 \times 10^{-7}\text{ m}^2 \cdot \text{s}^{-1}$ and the experimental curve (residuals) are also shown in Fig. 2. The analysis of residuals is a powerful tool for checking the experimental data. From the distribution of the residuals in this particular case, it is clear that the experiment was conducted correctly and the mathematical model used in the direct heat conduction problem is close to reality. Multiple thermal-diffusivity measurements are made at each temperature level, and average values are reported.

2.2.3 Uncertainty

The uncertainty of the 3P method was determined in accordance with the *ISO Guide to the Expression of Uncertainty of Measurement* [14]. All possible sources of uncertainty can be distributed into five major categories:

(1) Measurement Means

This category represents the devices used for the measurement of the physical quantities involved in the determination of the thermal diffusivity (sample thickness, thermocouple positions, voltages delivered by the thermocouples, time, baseline temperature value, baseline stability).

(2) Method

Uncertainties were mainly due to the differences between experimental conditions and the assumptions upon which the model of the method was based. Badly controlled initial and boundary conditions, especially non-constant sample temperature before the thermal disturbance, two- or three-dimensional heat flow in the sample, multi-component heat flow in the sample (radiation and convection), represent significant sources of uncertainty. Optimally designed experiments can minimize these effects.

(3) Material

Uncertainties related to the geometrical quality of the sample (optimal sample thickness, flatness and parallelism of the surfaces) and its chemical, optical, and thermophysical properties (isotropy, homogeneity, opacity, etc.). The sample dimensions are measured using a calibrated micrometer at room temperature. An additional uncertainty due to sample and sample holder thermal expansion has to be taken into account above room temperature. Thermal insulation materials are often highly anisotropic, inhomogeneous, and translucent; therefore, uncertainties due to radiative and convective heat transfer often pose a serious problem.

(4) Surroundings

The uncertainty sources related to the sample boundary conditions arising from the furnace design, especially the furnace temperature homogeneity and stability. The nature of the atmosphere (inert gas at certain pressure, or vacuum) can also contribute to excessive heat losses and sample temperature fluctuations. The baseline temperature uncertainty due to instability during the measurement can be prevented by a good furnace design and careful temperature stabilization during the experiment. The uncertainty is usually higher at high temperatures due to higher signal-to-noise ratio and furnace temperature fluctuations, especially when measured in gas atmospheres at higher pressures.

(5) User

The uncertainty in this category depends on the operator's skills and expertise. The sources are related mainly to the quality of the sample preparation, attaching and inserting the thermocouples, the selection of the time limit for the experiment, and the correction for the sample baseline temperature drift.

The relative expanded uncertainty (coverage factor $k = 2$) of the thermal diffusivity determination $U_r(a)$ is estimated to be from $\pm 6\%$ to $\pm 15\%$, depending on material and temperature. The uncertainty components having the most weight are those related to sample thickness, thermocouple positions, baseline drift, and (at higher temperatures) those related to multicomponent heat transfer in the sample.

Since the thermal conductivity λ is the product of the thermal diffusivity, the specific heat, and the density, the combined relative expanded uncertainty of the

thermal-conductivity determination $U_{C,r}(\lambda)$ is given by

$$U_{C,r}^2(\lambda) = U_r^2(a) + U_r^2(c_p) + U_r^2(\rho). \quad (8)$$

The relative expanded uncertainty of the specific heat determination $U_r(c_p)$ by using differential scanning calorimetry (DSC) is estimated to be $\pm 5\%$ and the relative expanded uncertainty of the density $U_r(\rho)$ is $\pm 3\%$. The combined relative expanded uncertainty of the thermal-conductivity determination is, therefore, estimated to be from $\pm 8.4\%$ to $\pm 16.1\%$.

2.3 Comparison with Steady-State Methods

The modified step heat technique was used by Rooke and Taylor [8] to determine the diffusivity and the conductivity of thermal insulation standard materials, e.g., SRM 1450b, Ceraboard 141, Carborundum Fiberfax 3000 (FF), and C.E. Refractories Cerwool 2300.

Later, Taylor [9] reported the thermal diffusivity/conductivity measurements of a number of insulating materials (e.g., felts, rubbers, ceramic foams, fiberglass fiber rolls, thermal barrier coatings, and multi-layer insulation) and showed that the results were in good agreement with those obtained by other techniques.

Since that time, we have used the technique to measure a great variety of other insulating materials. These include aerogels, metallic foams, micro- and nano-porous insulation, and carbon fiber insulation. Most of these measurements involved proprietary materials so the results were not published. Thus, the wide-scale use of this technique has not been known to the general technical community.

Some typical results for the thermal-diffusivity measurements on the micro-porous insulation material Microtherm HT in a mixture of helium and argon gas at normal atmospheric pressure are shown in Fig. 3. Corresponding thermal conductivity values are shown in Fig. 4. Low thermal conductivities of the micro-porous materials are due to their mechanical structure with pore diameters below $0.1 \mu\text{m}$. This leads to the reduction of the gas conduction contribution to the total heat transfer rate, with a negligibly higher portion of solid conduction. At higher temperatures ($T > 350^\circ\text{C}$), radiation becomes the main heat transfer mechanism in the material. For optically dense porous materials, the effective thermal conductivity λ_{eff} can be expressed in terms of the local radiation temperature T_R as [15]

$$\lambda_{\text{eff}} = \lambda_c + \frac{16}{3} \frac{n^2}{\beta} \sigma T_R^3, \quad (9)$$

where λ_c is the effective thermal conductivity due to the gas and solid conduction, n is the index of refraction ($n \approx 1$), σ is the Stefan-Boltzman constant, and β is the gray extinction coefficient. The second term in Eq. 9 represents “radiative conductivity” based on the Rosseland diffusion approximation. Plotting the effective thermal conductivity as a function of T_R^3 should result in a linear representation that allows determination of β from the slope of the linear portion. Graphs of thermal conductivity

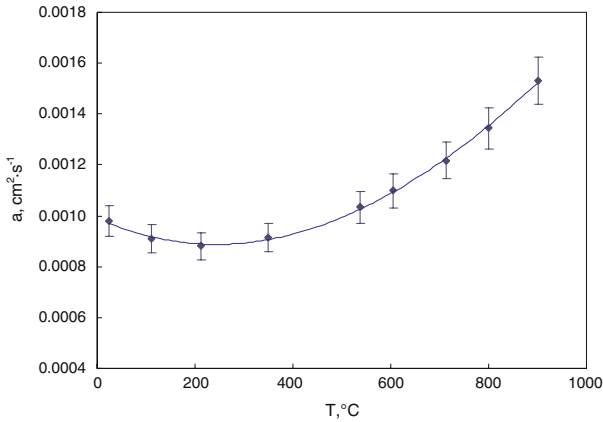


Fig. 3 Thermal diffusivity of Microtherm HT

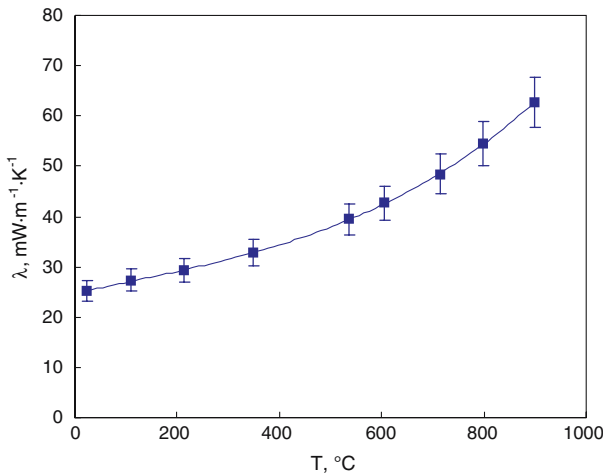


Fig. 4 Thermal conductivity of Microtherm HT

as a function of T_R^3 for Microtherm HT are shown in Fig. 5. The calculated value of the gray Rosseland extinction coefficient is $\beta = 1.40 \times 10^4 \text{ m}^{-1}$.

In order to check the results with a steady-state method, the thermal conductivity of Microtherm HT (sample diameter $\varnothing = 48.65 \text{ mm}$, thickness $L = 4.074 \text{ mm}$, mass $M = 2.5960 \text{ g}$, and density $\rho = 342.8 \text{ kg} \cdot \text{m}^{-3}$) was measured in air at normal pressure and room temperature by the 3P method and also by the heat flow meter technique [16]. The specific heat of the sample material was measured by differential-scanning calorimetry (ASTM Standard E-1269). The results of the thermal-conductivity determination are listed in Table 1. The difference between the two thermal conductivity values was less than 1%.

Another interesting material that has been measured is an adhesively bonded honeycomb-core panel [17]. The honeycomb-core panel was made of titanium alloy

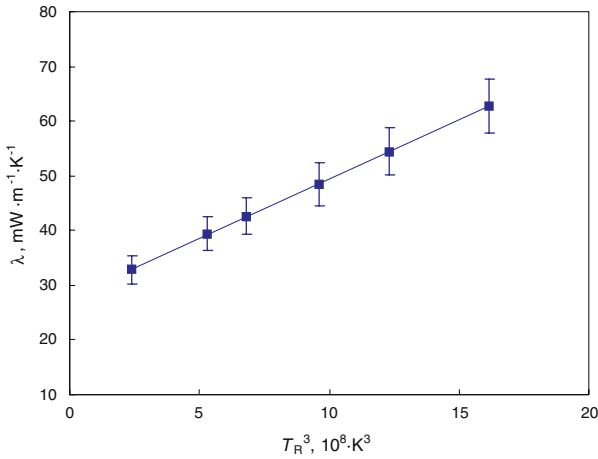


Fig. 5 Thermal conductivity of Microtherm HT as a function of T_R^3

Table 1 Thermal-conductivity results for Microtherm HT at room temperature in air at normal pressure

Method	Density ($kg \cdot m^{-3}$)	Thermal diffusivity ($mm^2 \cdot s^{-1}$)	Specific heat ($J \cdot g^{-1} \cdot K^{-1}$)	Thermal conductivity ($mW \cdot m^{-1} \cdot K^{-1}$)
3P	342.8 ± 10.3	0.108 ± 0.006	0.703 ± 0.035	26.0 ± 2.2
Heat flow meter	342.8 ± 10.3			25.8 ± 2.1

with a density of $94.5 kg \cdot m^{-3}$. The core was 25.4 mm thick and consisted of 4.76 mm non-corrugated hexagonal cells with 0.035 mm foil thickness. The face sheets were made of titanium and were 1.6 mm thick. The honeycomb core was attached to the face sheets using a modified epoxy adhesive film supported by a polyester knit fabric. Two layers of the adhesive at $0.49 kg \cdot m^{-3}$ were applied to each face sheet. The adhesive thickness was 0.94 mm.

The effective thermal diffusivity of the honeycomb core structure was measured using the 3P technique over the temperature range from room temperature to 200 °C. The resulting thermal conductivity values are shown in Fig. 6. The same core structure was also measured using two different steady-state techniques at three different laboratories. Two laboratories utilized the GHP technique; one laboratory used the heat flow meter apparatus. All the measurements were performed on a 203.2 mm diameter specimen, except for the 3P technique which used a 203.2 mm diameter specimen for the room-temperature measurement and a 50.8 mm diameter specimen for measurements above room temperature. The results from the steady-state experiments were all up to 50% higher than those for the 3P technique.

Since the honeycomb structure core is a highly inhomogeneous material, the results of the transient measurements, based on the concept of the thermal diffusivity, could be questioned. In order to theoretically verify the results, the combined steady-state radiative and conductive heat transfer in the honeycomb core panel was modeled

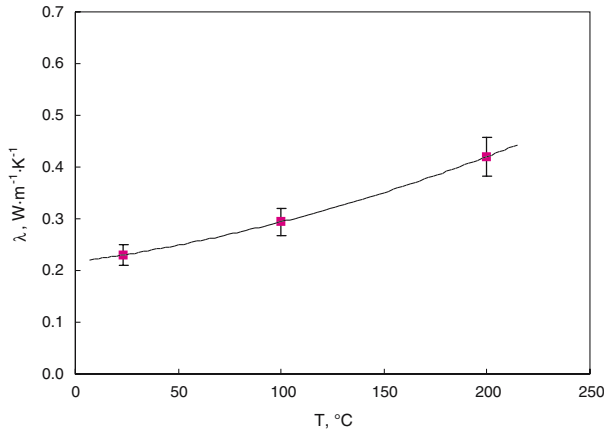


Fig. 6 Thermal conductivity of honeycomb core panel

Table 2 Average difference of various experimental data with respect to average predictions by the finite-volume numerical model [18]

Measurement technique	Average difference (%)
GHP-1	38.0 ± 18.1
GHP-2	47.3 ± 11.1
Heat flow meter	12.9 ± 26.8
3P	1.7 ± 5.9

using a finite-volume numerical formulation [18]. The nonlinear governing equations were solved using a modified Newton-Raphson method. The effective thermal conductivities were calculated from the converged steady-state solutions of the numerical finite-volume model using a thermal conductivity of adhesive-to-air ratios of 10 and 100. A comparison of the calculated effective thermal-conductivity values with the experimentally obtained data is given in Table 2. The transient 3P experimental data were found to be in best agreement with the numerical finite-volume predictions with a difference of $1.7 \pm 5.9\%$. These results do not in any way question the validity of the steady-state techniques, but imply that the measurements obtained for the samples were not accurate [18].

3 Conclusion

The use of faster transient techniques to determine the thermal diffusivity/conductivity of insulating materials is increasing and this trend will continue. Further development of the transient 3P method for the thermal diffusivity measurement of thermal insulations is described in detail in this article. Mathematical approximations for boundary conditions in the former step-heat method were replaced by measured time–temperature curves at the sample boundaries and a new, stable DHW algorithm replaced the old finite-difference scheme used to solve the direct heat conduction problem. The apparatus was also modernized, and the temperature range of the

measurement was increased from -120 to 900 °C. The method was successfully tested for diffusivity measurements of highly anisotropic, extremely low conductive, and inhomogeneous materials, such as honeycomb structures, aerogels, and micro-porous insulations.

References

1. ASTM Standard C177-04, *Standard Test Method for Steady-state Heat Flux Measurements and Thermal Transmission Properties by Means of the Guarded-Hot-Plate Apparatus*. (ASTM, Philadelphia, 2004)
2. ASTM Standard C518-04, *Standard Test Method for Steady-state Thermal Transmission Properties by Means of the Heat Flow Meter Apparatus*. (ASTM, Philadelphia, 2004)
3. ISO Standard 8301, *Thermal Insulation, Determination of Steady-state Thermal Resistance and Related Properties, Heat Flow Meter Apparatus*. (ISO, Geneva, Switzerland, 1991)
4. R.E. Taylor, J. Gembarovic, K.D. Maglic, in *Characterization of Materials*, vol. 1, ed. by E.N. Kaufman (John Wiley & Sons, New York, 2003), p. 663
5. P. Andersson, G. Backstrom, *Rev. Sci. Instrum.* **47**, 205 (1976)
6. S.E. Gustafsson, *Rev. Sci. Instrum.* **62**, 797 (1991)
7. R.R. Bittle, R.E. Taylor, in *Thermal Conductivity 18*, ed. by R. Ashworth, D.R. Smith (Plenum, New York, 1984), pp. 379–390
8. S.P. Rooke, R.E. Taylor, *J. Heat Transfer-Trans. ASME* **110**, 270 (1988)
9. R.E. Taylor, in *Thermal Conductivity 22*, ed. by T.W. Tong (Technomic Pub. Co., Lancaster, Pennsylvania, 1994), pp. 567–578
10. H.S. Carslaw, J. C. Jaeger, *Conduction of Heat in Solids*, 2nd edn. (Oxford Univ. Press, New York, 1959), p. 103
11. J. Gembarovic, M. Loffler, J. Gembarovic Jr., *Appl. Math. Model.* **28**, 173 (2004)
12. M. Loffler, J. Gembarovic, J. Gembarovic Jr., in *Thermal Conductivity 26/Thermal Expansion 14*, ed. by R.B. Dinwiddie, R. Mannello (DEStech Pubs., Lancaster, Pennsylvania, 2005), pp. 123–133
13. P.T. Boggs, J.R. Donaldson, R.H. Byrd, R.B. Schnabel, *ACM Trans. Math. Software* **15**, 348 (1989)
14. *ISO Guide to the Expression of Uncertainty in Measurements* (ISO, Geneva, Switzerland, 1995)
15. M. Spinnler, E.R.F. Winter, R. Viskanta, *Int. J. Heat Mass Transfer* **47**, 1305 (2004)
16. K. Collins, *Thermal Conductivity Test Report* (LaserComp, Inc., Saugus, Massachusetts, 2003), p. 1
17. K. Daryabeigi, Heat Transfer in Adhesively Bonded Honeycomb Core Panel. *AIAA Paper 2001-2825* (2001)
18. K. Daryabeigi, *J. Thermophys. Heat Transfer* **16**, 217 (2002)